

## Disparity of ground-based Total Solar eclipse polar plumes and AIA/SDO space mission EUV ray-like jets

Heydari, M.<sup>1</sup>  | Tavabi, E.<sup>1</sup>  

1. Department of Physics, Payame Noor University (PNU), Tehran, Iran.

Corresponding Author E-mail: [e\\_tavabi@pnu.ac.ir](mailto:e_tavabi@pnu.ac.ir)

(Received: 15 April 2023, Revised: 15 May 2023, Accepted: 26 Sep 2023, Published online: 20 Feb 2024)

### Abstract

Multi-wavelength observations could help discriminate the fundamental differences for the mechanism of the jet-like structures of the hot and cool material in the inner atmosphere. We use the *Atmospheric Imaging Assembly (AIA)* on-board the *Solar Dynamics Observatory (SDO)* for unprecedented temporal and spatial resolving power for a wide range of wavelengths to increase our knowledge about the origin and the evolution of jets. The dynamical behavior of the jets in polar plumes (PP's) is considered for the first time based on the simultaneously observed in space EUV hot, and cool emission lines also observed in W-L at total eclipses.

At the USA 2017 total solar eclipse, we observed white-light polar plumes (W-L PPs) with an excellent resolution from different sites. We tried several combinations of pictures taken (a) from different sites on the ground, using different image processing (techniques), and (b) from space, taken with different coronal filters and time sequences. The resolution of the faint polar regions space images are of low signal/noise (S/N) ratio, and instead of summing pixels of images to reduce the noise of individual images, we found it more efficient to sum a burst of 5 to 10 min consecutive AIA frames from a sequence taken around the total eclipse time. This should smear out the fast dynamical events showing fast dynamical events, but the jet part is not significantly smeared, as the flow being linear. We also found promising results using the 171 Å filter with temperature sensitivity extended from 0.6 MK to 2 MK due to lines of Fe IX, Fe X and Ni XIV but also performed the analysis with the higher temperature sensitivity filters, at 193 and 211 Å. The relationships of W-L PP's with inner parts off-limb EUV emission lines jet-like structures demonstrated a highly correlated behavior. In most cases, we found a cross-correlation coefficient in order of 85% in coronal hole regions; however, this correlation is not perfect in some cases. Therefore, in these features, the direct connection was not detectable obviously, the disparity could be related to Doppler dimming effect in high velocity jet like plums. However, most W-L plumes have counterparts with EUV ray.

**Keywords:** Total eclipse, Corona, Polar plume, Polar-rays.

### 1. Introduction

The appearance of the solar corona over the poles during times of low solar activity is dominated by the presence of polar plumes. Their well-known resemblance to the lines of force about a dipole suggests that plumes represent tubes of elevated coronal density confined by the magnetic fields. Then, the relative isolation of plumes and the possibility of their identification separate from any background corona, presents a unique opportunity to discover how the corona's structure may be influenced by changes in the underlying chromosphere and transition region and their magnetic fields. The primary purpose of this analysis is to determine what connection exists between

inner plumes, elongated outer plumes, and the relationship of inter-plumes with the fast solar wind.

Earlier investigators (e.g., Van De Hulst, 1950; Saito, 1965) have identified particular features over the poles as plumes and then have described their photometric physical properties and spatial distribution. Such studies inevitably require an undesirable, subjective choice of which features are significant and to be identified as polar plumes. In addition, the resultant ambiguity partly accounts for the lack of agreement concerning such parameters as their mean diameter.

Del Zanna et al. (2003) found that bright

Cite this article: Heydari, M., & Tavabi, E. (2024). Disparity of ground-based Total Solar eclipse polar plumes and AIA/SDO space mission EUV ray-like jets. *Journal of the Earth and Space Physics*, 49(4), 161-173. DOI: <http://doi.org/10.22059/jesphys.2023.357385.1007515>

E-mail: (1) [mehri.heidari.zanjan@gmail.com](mailto:mehri.heidari.zanjan@gmail.com)



Publisher: University of Tehran Press.

DOI: <http://doi.org/10.22059/jesphys.2023.357385.1007515>

Print ISSN: 2538-371X  
Online ISSN: 2538-3906

points were seen near the plume footpoints only in the early phase of their formation. Wilhelm et al. (2010) found a strong association of plumes and jets from XRT/Hinode images, and Raouafi et al. (2007) showed that X-ray jets were precursors of coronal plume formation.

Polar plumes or polar rays are thinner structures in the white-light corona that have been observed since 19<sup>th</sup> century, in fact, regarded as a first firm proof of the existence of the global magnetic fields of the Sun. They are predominantly observed around the poles during the minimum of solar magnetic cycle, projecting onto a relatively darker background that consists of coronal holes/cavities. The polar plumes or rays are thread-like thin, long, open magnetic tubes whose average density is 2–4 times greater than that in the surrounding medium, about  $3 \times 10^6 \text{ cm}^{-3}$ , whose a typical temperature at the base is in the order of  $1.2 \times 10^6 \text{ K}$ , as inferred by Saito (1965, and references therein) from eclipse observations. These values have subsequently been confirmed by space-borne observations, e.g., by Ko et al. (2022), Muglach (2021) and review paper by Poletto (2015), who were among the first to analyze EUV observations of these structures. Pasachoff et al. (2009) showed that an outward propagating brightening have been detected with speeds in the range 32 – 146 km/s; higher speed is also reported by Il-Hyun Cho et al. (2019). They show an average speed at their maximum heights is found to be  $132 \pm 44 \text{ km/s}$  ranging from 57 to 264 km/s along the propagation direction. The average lifetime is  $20 \pm 6$  ranging from 11 to 36 s.

Tavabi et al. (2018) illustrated the temporal evolution from the 304 Å images of the tornado, the main components (or kernels) of the event are launched from the base with a constant proper velocity having an average value of  $140 \pm 40 \text{ km s}^{-1}$ , and a rotational velocity with a similar value, of  $145 \text{ km s}^{-1}$  in this cold line. Their filtering process allows us to separate short-lived dynamic phenomena from rather longer life-time background plume intensity variations. The time-distance diagram along the axis of tornado in 304 Å line suggests that later the ejected plasma is flowing back to the Sun. This type of suggested complete parabola motion path is not seen in the 193 Å line. The

longitudinal motion observed is confirmed by the enhancement appearing later above the same polar region and the same radial position, over the occulting disk of the C2 coronagraph of LASCO. They also found that the ejection of the cold He II plasma is delayed by about 4 min in the lowest layer and more than 12 min in the highest level compared to the hot 193 Å behavior. Wang et al. (1998) already reported a large correlation between the Extreme-ultraviolet Imaging Telescope (EIT) jets and the long narrow white light structures in the outer corona recorded using the LASCO observations, as well as a large maximum value of velocity, in the order of  $1100 \text{ km s}^{-1}$  for the leading edge of the white-light jets.

Gupta et al. (2010) propose that interplume regions host Alfvénic or fast magnetoacoustic waves, while waves in plumes are likely of the magnetoacoustic type. Moreover, the observed acceleration of interplume waves makes them good carriers for transporting energy to the outer coronal layers. However, the propagation speed is markedly higher in interplumes (where it increases from about  $130 \text{ km s}^{-1}$  just above the limb to about  $330 \pm 140 \text{ km s}^{-1}$ , at 160 arcsec above the limb) than in plumes, where, the speed, although having about the same value, at the lower level, only rises to about  $165 \text{ km s}^{-1}$ .

Pant et al. (2015) established a significant relationship between the IRIS small-scale jets originating in network lanes and plumes. They found evidence of outflows at the bases of plumes from the average Doppler displacement (see also Jiao et al., 2015).

Several observations have been performed during total solar eclipses for the detection of “high-frequency coronal waves” using the visible emission lines, but their origin remains elusive (Koutchmy and Stellmacher, 1976; Samanta et al., 2015); however, to reveal the importance of the mechanism causing high-frequency oscillations. The events were simultaneously observed in a time sequence of data obtained at multiple EUV wavelengths. In order to understand their dynamical characteristics with the combination of WL eclipse data, larger distance from solar limb should be taken into the account (Tavabi et al., 2018). Samanta et al. (2015) implemented the multi-slit spectroscopic observations during the 2010

total solar eclipse for looking at high-frequency oscillations along the plumes and found a typical period of 10 s, that could contribute significantly in the heating of the corona. The longer periods up to 25 have been reported by Gupta et al. (2010), using the spectral diagnostic capabilities of the SUMER spectrograph, and with a rigorous statistical approach, evidence for propagating magneto-acoustic waves in polar coronal hole regions have been found.

Banerjee et al. (2009a) using the Extreme ultraviolet Imaging Spectrometer (EIS) onboard Hinode, found the nonthermal velocity was inversely proportional to the quadratic root of the electron density, in excellent agreement with what was predicted for undamped radially propagating linear Alfvén waves. They studied the plumes and interplumes non-thermal velocity with height above the limb from the Fe XII 195 Å line, by HINODEH EIS spectrograph, accompany with SUMER Si VIII 1445.75 Å line. They found obvious evidence for upwarding Alfvén waves, and illustrated the width of the lines getting weaker after the height about of  $1.1R_{\text{sun}}$ . In addition, the effective electron temperatures rise to  $20 \times 10^6$  K in the darkest region of interplumes area, and the line width is much broader in interplumes.

The larger widths in the interplume regions as compared to plumes, indicate that perhaps interplumes are the preferred channel for the acceleration of the wind.

Also the presence of longer period oscillations with periods of 10 to 30 min in polar coronal holes with oscillations have an amplitude of a few percent in radiance and are not detectable in line-of-sight velocity for propagating velocities from  $75 \text{ km s}^{-1}$  (Ne VIII) to  $125 \text{ km s}^{-1}$  (Fe XII) that have been reported by Banerjee et al. (2009b).

The contribution of polar plumes to the fast solar wind rising from the polar CH is thus still a subject of debate and controversy (e.g. Habbal, 2010; Gabriel et al., 2005). More details about plumes and inter-plume regions were listed in the review of Wilhelm et al. (2011) and of Poletto (2015).

To make a more objective study, we have performed a detailed comparative analysis of the W-L radiance of the outer corona above the pole during the total solar eclipse with the AIA/SDO filtergrams at inner CH regions. The dominant correlation

components of the composite images are used to infer the ambiguity distribution within a CH region plume and are used to discover what connection exists between polar inter-plumes and fast solar wind acceleration.

## 2. Observations and Data Reduction

The primary data for this study was the eclipse W-L made during 2017, of the last minimum solar cycle data recorded using the CMOS cameras of the Institute d'Astrophysique de Paris (IAP experiments run at Indian Valley (Idaho - 17:27 UT) seen as Figure 1, and with another imaging group in Oregon (17:12 UT).

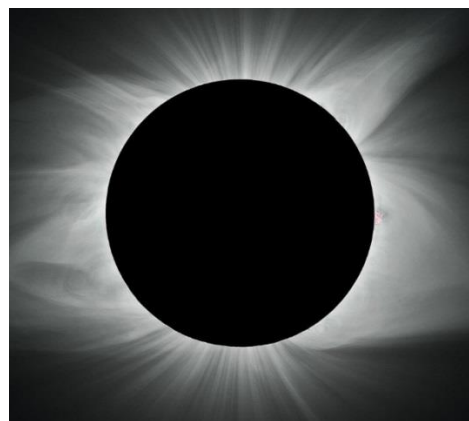


**Figure 1.** W-L image on August 21, 2017 total solar eclipse at 17:24 UT, Idaho, USA, (Courtesy to J. Mouette, the IAP eclipse team).

The AIA/SDO is four different array telescopes that capture the frames of the Sun's transition regions and corona out to  $\sim 1.3 R_{\text{sun}}$  in 10 separate EUV and UV channels (Title et al., 2006). The images are  $4096 \times 4096$  square with a pixel size of  $0''6$  in the full spatial resolution mode, with a cadence of 12 s (in EUV filtergrams and for UV channels observe with a cadence of 24 s, Lemen et al., 2012) on August 2017, 21.

Figure 2, panel (a), the inner part (Fe IX 171 Å), and panel (d), illustrate the AIA images correspond to 150 frames with a 12 s cadence after summing intensities between and after unsharp masking. Intensities are in the logarithmic scale for Fe XII 193 Å, Fe IX 171 Å, and at the bottom for He II 304 Å in polar coordinate. An extended sequence was prepared for the analysis of Coronal Hole Polar Plumes (CH PP's) at the time of the total solar eclipse of 2017 to enhance the S/N ratio and to improve the visibility of tiny PP's. The processing method is implemented on

frame summing, radial filtering, and typical unsharp masking. To increase the S/N ratio, the successive frames are added, the radial filtering directly operates on the corrupted reconstructed image, to effectively and efficiently reduce artifacts. The filter adapts to the severity of local artifacts to preserve spatial resolution as much as possible. The widths and direction of the filter are derived from the local structure. Visual inspection shows that this radial adaptive filter is superior with the respect to existing methods in the case of mildly distorted images. The unsharp masking is a technique in which an image is sharpened by subtracting a blurred (unsharp) version of the image from itself.

Tavabi et al. (2018) used the EUV observations from a sequence of data at polar CH plumes with ray-like jets to show the evidence of longitudinal acceleration in the partial emissions of the 1.25 MK line of Fe XII at 193 Å and others. The structures along the plume intermittently show a propagating outward velocity of about 140 km/s interpreted as an upwards propagating wave in the HeII 304 Å and the coronal Fe IX lines; higher speeds are recorded in the hotter Fe XII line (up to 1000 km/s). A space-time plot reveals that a large amount of the fast-ejected material originates from below the PP.

Finally, they found a temporal and spatial relationship between the cool and hot components of the tornado-like ejection. No evidence of PP providing a large amount of material for the fast wind is apparent.

Here, the fast rays of the W-L eclipse (Figure 1) and without the counterparts in EUV's, were occurring in the north CH on August 21, 2017, showing new details better than illustrated before.

### 3. Data Analysis

In the attempt to resolve the ambiguities of the uncorrelated terms of the W-L polar plumes and AIA filtergrams traced of PPs, we have constructed the composite image at the solar radii which is about  $1.3R_{\text{sun}}$ . The correspondence (and un-correspondence) between the W-L plumes and AIA plumes was marked by arrows (with different colors), which gives confidence that the differences are genuinely representative in Figure 2 left down panel and Figure 3 as magnified. The orange arrows show the un-

correlated cases with AIA channels, while the pink arrows for the W-L counterparts of AIA emission PPs (also see Figure 8 for more details). In Figure 4, the intensity around the  $1.3R_{\text{sun}}$  is illustrated for 171 Å and W-L for full disk (top panel), the middle and bottom graphs give the CHs with better visibility. To have a better comparative view, the subsection marked by horizontal double head dashed arrows in Figure 4, was replotted in Figure 5. The peaks of intensity for AIA emission and eclipse scattered light show a typical correlation with significantly high correlation coefficients ( $83 \pm 5$  percent). The same behavior was also seen for 193 Å in Figure 6 for the full disk in similar radial distance with correlation coefficients of about of  $86 \pm 5$  percent.

Images are highly processed (e.g., see Habbal et al., 2010; Pasachoff et al., 2009) to increase the contrast and visibility of ray-like linear details called polar rays to search for the sources of the fast solar wind inside coronal holes (CH). Small scale explosive events resulting from magnetic reconnections (Tavabi et al., 2015) are believed to produce linear jets, possibly propelling and heating the CH plasma (e.g., Sterling et al., 2015) towards the high corona following the open magnetic field lines of Polar Regions. Past eclipse observations suggested that W-L PPs reflect the process, but no precise correlation analysis implying the coronal surface events and the eclipse W-L images was attempted. The space observations of the corona using the EUV/SDO fast imaging instruments (Title et al., 2006) permit finding a precise correlation of the surface EUV brightening events, including minute loops and jets near the limb, with the eclipse polar rays from processed pictures (see more details in Tavabi et al., 2018). The 171 Å wavelength band is expected to observe the Fe ix 171.07 Å line [ $\log T \sim 5.85$ ] for quiet Sun observations. For CH plasma, the dominant contribution comes from the Fe ix 171.07 Å line. For the flare spectrum, the dominant contribution comes from the Fe ix 171.07 Å line, with a more contribution from continuum intensity. The 171 Å channel has a response to flare-like temperatures due to Fe xx lines. The 193 Å passband is dominated by Fe xii lines [ $\log T \sim 6.2$ ] for disk observations. For the quiet Sun

and active region spectra, the main contribution is due to Fe xii lines, but with a peak of contribution from Fe xi lines. In flaring events, the 193 Å channel is dominantly contributed by the Fe xxiv 192.03 Å line [ $\log T \sim 7.25$ ]. However, for the CH regions, there are expected to have Fe ix, Fexi, and Fe xii lines, also

the 211 Å passband is included in the Fe xiv 211.32 Å line [ $\log T \sim 6.3$ ] for the active region (O'Dwyer et al., 2010). However, no filtergram is expected to be purely isothermal, meanwhile that emission from ionized gas formed at a wide range of temperatures responds to the total emission irradiance.

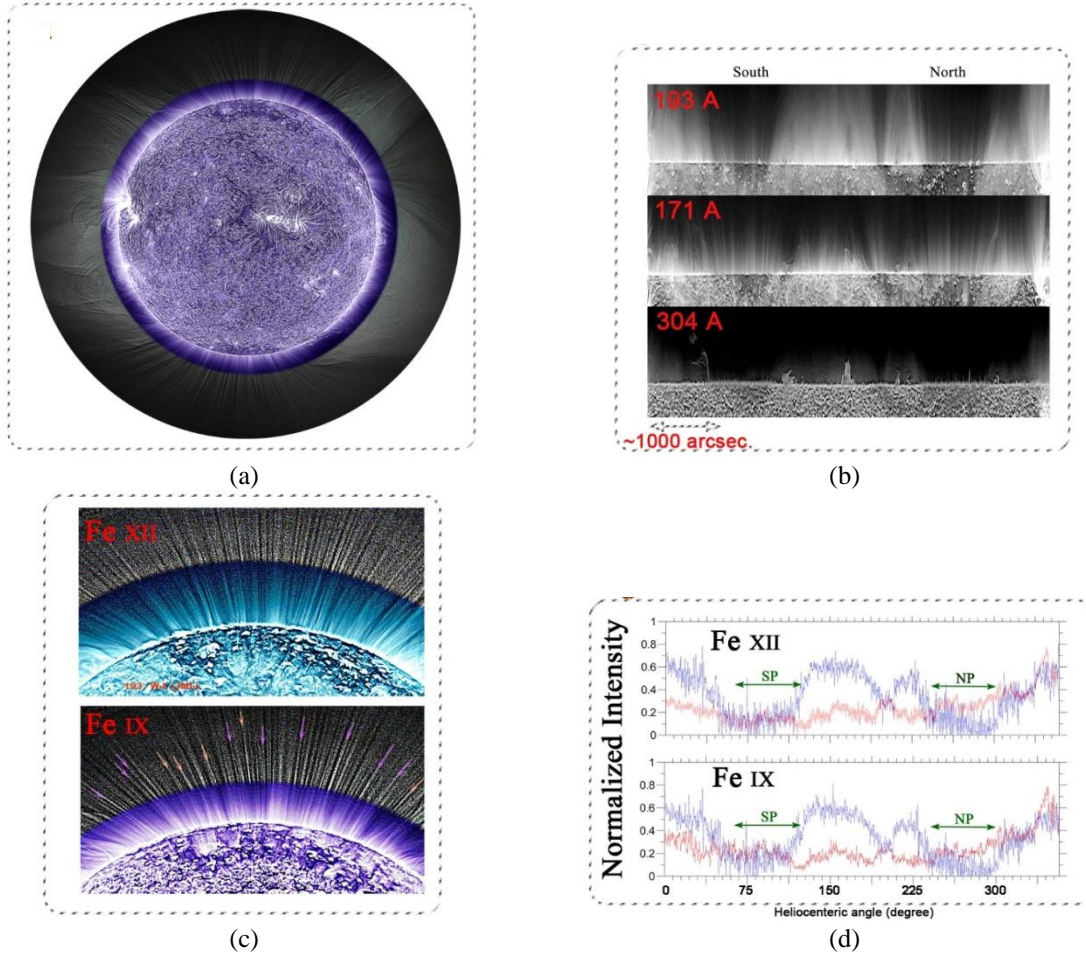


**Figure 2.** a) A composite WL eclipse image with highly processed AIA/SDO 171 Å (inner part), b) 193, a171, 304 Å filtergrams of AIA in polar coordinate, c) again two composite images in 193 Å (Fe XII) and 171 Å (Fe IX) in north CH, and d) the full disk relative intensity profiles above the limb at 1.3 solar radii in WL and AIA two channels.

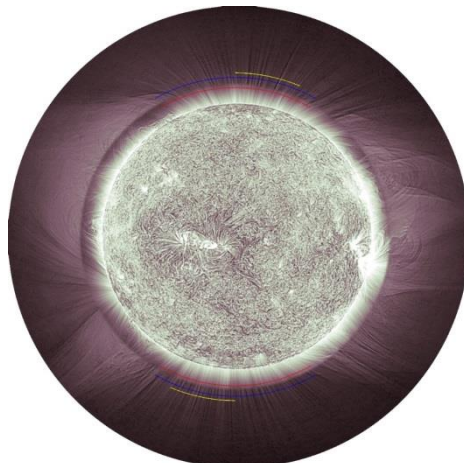


**Figure 3.** As Figure 1-a panel with larger size, the red, blue, and yellow lines show the region that will consider as the following Figures, the inner part corresponds to 171 Å summed image.

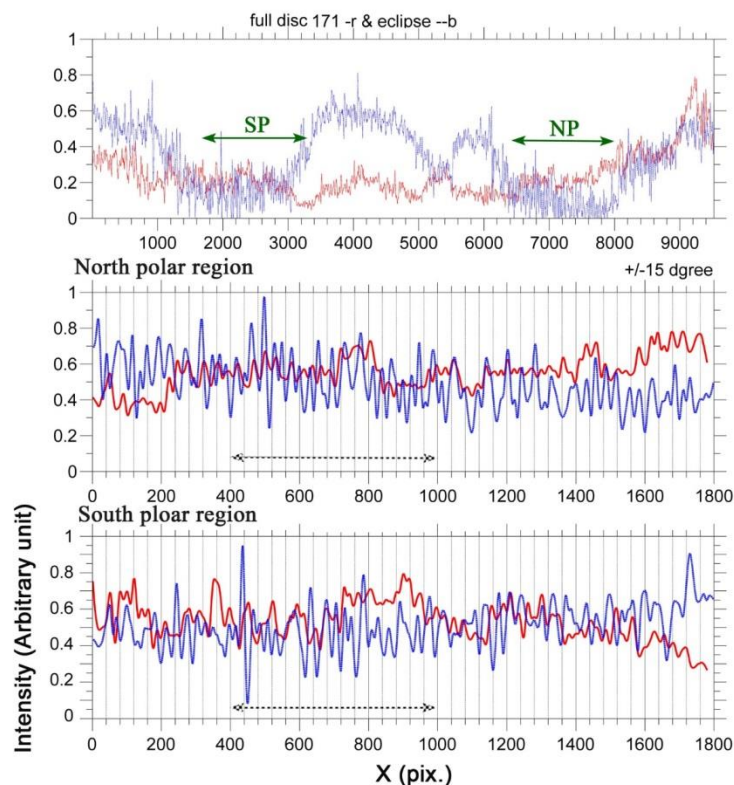


**Figure 4.** The CH poles, as shown in Figure 3 as solid red (AIA) and dotted blue (WL eclipse) curves that are cover +/- 15 degrees of polar regions and marked as green arrows at the top panel. The AIA 171 Å line and W-L profiles with a cross-correlation coefficient is about of 83 percent in CH's. The dotted arrows are seen as yellow curve and will be replotted as the following figure.

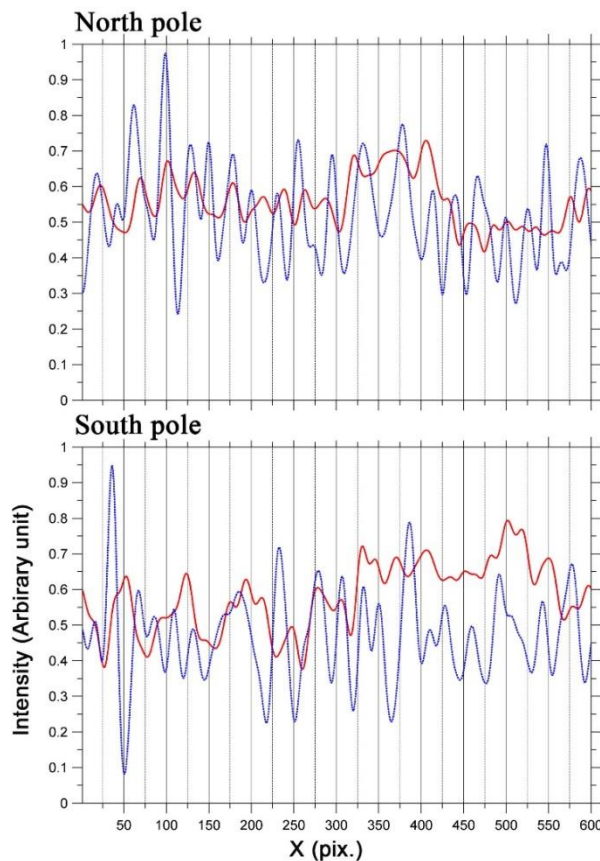


**Figure 5.** Red solid line for eclipse W-L, and the dotted line is the intensity profile of AIA 171 Å, inside the N&S poles, the regions correspond to dark dotted arrows in Figure 4.

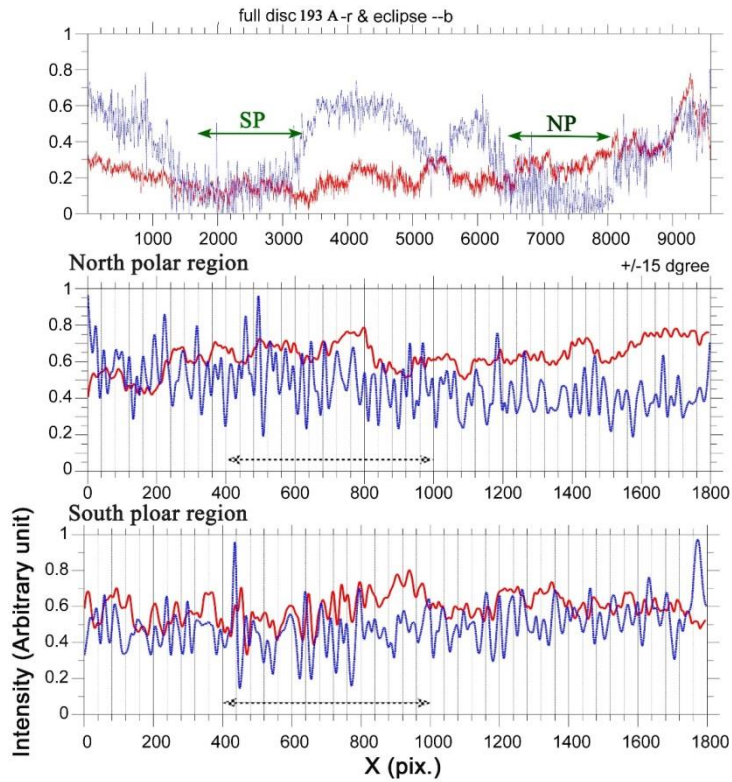


**Figure 6.** The CH poles as shown in Figure 3, as solid red (AIA) and dotted blue (WL eclipse) curves that cover +/-15 degrees of polar regions and marked as green arrows at the top panel. The AIA 193 Å line and W-L profiles with a cross-correlation coefficient is about of 86 percent in CH's. The dotted arrows are seen as yellow curve, and will be replotted as the following figure.

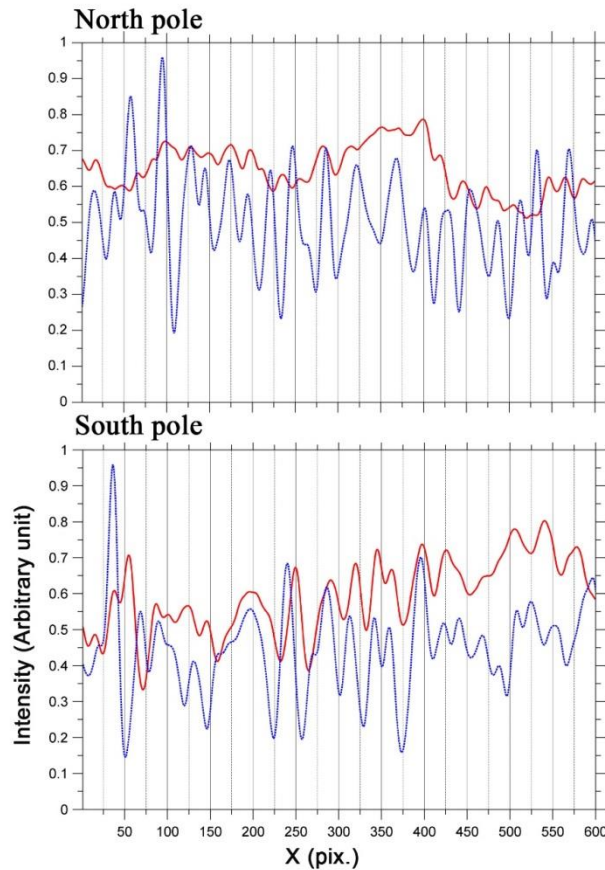


**Figure 7.** Red solid line for eclipse W-L, and the dotted line is the intensity profile of AIA 193 Å, inside the N&S poles, the regions correspond to dark dotted arrows in Figure 6.

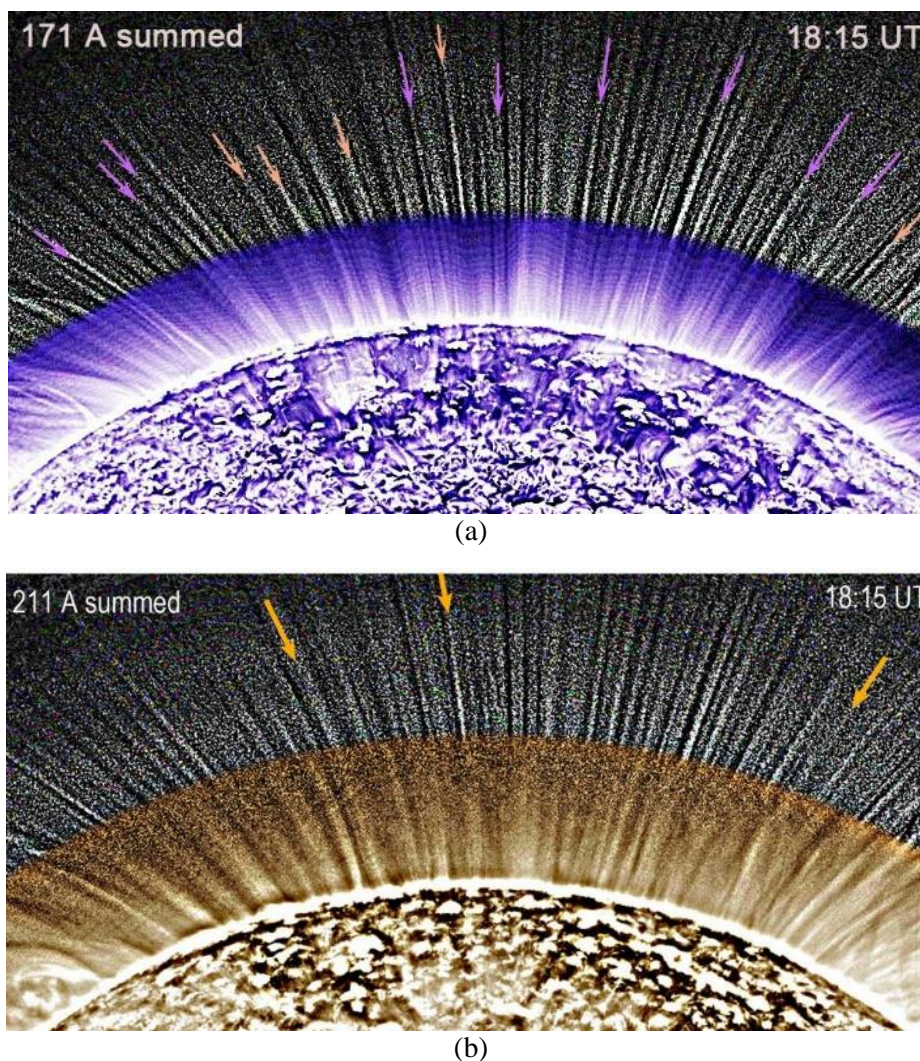


**Figure 8.** The inner parts are the summed images for 10 min. with a cadence of 12 sec. in 171 Å (a) and 211 Å (b), the outer part is highly processed to increase the S/N in the W-L eclipse image (18:15 UT). In panels, the yellow arrows indicate the uncorrelated rays.

All comparatively composite WL and AIA filtergrams (Figures 4 to 8), the AIA Fe IX 171 Å, relatively cool ( $\log(T) \sim 6$ ), and hotter lines (193 and 211 Å) demonstrate a high correlation coefficient with eclipse W-L intensity (Figures 4, 5, 6 and 7) that those dominated by the Thomson scattering mechanism, and their intensities are proportional to the square of  $n_e$ . However, some stealth W-L-PPs are seen without the emission correspondence (Figure 8, yellow arrows).

Figure 8 illustrates two typical results using a summed SDO images (171 Å and 211 Å) with an eclipse image from our set. Only the N- Pole region is reproduced in order to be capable to show the details.

#### 4. Results and Discussions

During the last half of the century, people

prepared tens and hundreds of papers and presentations dealing with the polar corona structure but mostly preferred to consider the polar corona homogeneous, for computing a model. Most inconsistent models are those considering a so-called "super-radial" expansion (Banaszkiewicz et al., 1998). They include the CH models where the confusion with SXR jets and transient (short life-time) extended polar jets are made (not to be confused with polar rays). Almost the SXR jets occur as the lambda shape configurations and as a result of magnetic reconnection, they are very dynamical and extend as magnetically confined plasma in a few minutes. Now, it is time to make a better analysis of PP's with taking into account: firstly, the existence of highly dynamical PP as slightly curved jets

with the fast outward motion and with short lifetime, like an impulsive phenomenon. Secondly, the much more stationary PP are frozen in the polar magnetic field (long lifetime polar rays), with  $T^\circ$  near one MK without significant outward velocities (indeed with the possibly slow downward flow); and finally with a background corona of very low density and unknown nature. Up to now, a long series of contradictory studies that comparatively look at the PP and interplume outward speeds, have been reported (e.g., Teriaca et al., 2003; Gabriel et al., 2005; Raouafi et al., 2007).

W-L polar plumes were observed for a long time at total solar eclipse near sunspot minimum, and it was clear that they have a higher density than the ambient background corona. Note that the densities in inter-plume regions are drastically lower than average densities of a polar region that includes PP, and being brighter in W-L than the interplume plasma. The unprecedented spatial resolution in both inner parts and outer parts of the corona, accordingly, could permit a better understanding of the plausible heterogeneous PPs in polar CH.

Pucci et al. (2014) illustrated that the population of the fast events was more petite in interplume regions, but there were otherwise no meaningful differences in the two plume and interplume distributions in the 171 and 193 Å filtergrams. They peak at the same speed (100 km/s) in the 193 Å channel and at a relatively lower speed (110 km/s vs. 167 km/s) in interplumes, with concerning plume value, in the 171 Å.

W-L rays are more extended than EUV plumes, because the Thomson scattered W-L irradiance depends linearly on the electron density  $ne$ , while the EUV emission depends on to square of the electron density  $ne$ . Koutchmy & Stellmacher (1976) found local densities in jet-like structures ten times over of the Van de Hulst model. Sornette et al. (1980) show that W-L plumes observed on the South Pole are the uppers of jets originating at the edge of the polar CH and are associated with the XUV bright points. We have solid pieces of evidence, which show that the inner corona bright points and jets are associated with the outer plumes; however, this scenario is not fully supported by other works such as Koutchmy and Bocchialini (1997) and Pasachoff et al.

(2009).

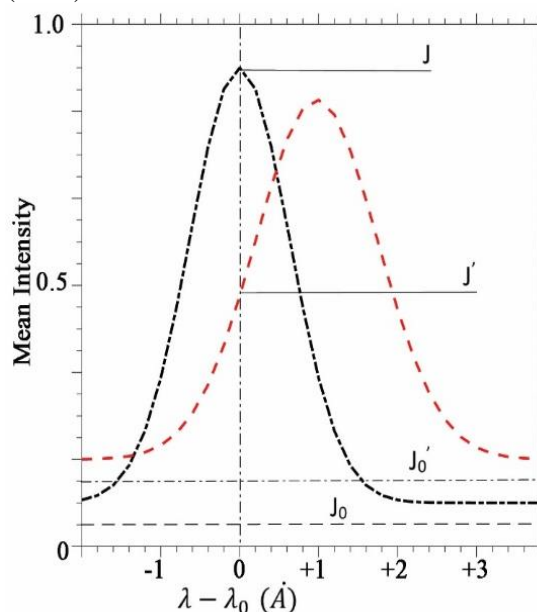


**Figure 9.** Scheme of the Doppler dimming effect in emission line profile to demonstrate the Doppler shift and dimmer the total intensity,  $J$  and  $J'$  show the peak of mean intensity (as seen by the scattering medium) for rest and dynamical parts.

Figure 9 describes this effect, namely, photoionization of a line by corona environment photons in a line center. This phenomenon extends to the so-called Doppler Dimming (DD), which can be described in the following way. In the case of the outward solar wind, the spectrum originating in the corona appears to be primarily redshifted. Hence, the photoionization rate of a coronal emission line depends on its quantity. If the wavelength displacement increases, then the peak of maximum intensity profile decreases drastically, and that would reach zero. When that amount is more extensive than the average of widths of the surrounding exiting line and the coronal absorption intensity profile, e.g.,  $\Delta\lambda = 0.5 \text{ \AA}$  at  $\lambda = 200 \text{ \AA}$ , which mainly belong to the most abundant coronal heavy ions, and includes the Fe IX and Fe XII, for an expansion speed of  $\sim 750 \text{ km/s}$ . This speed corresponds to the minimum amount of outflowing speed, which is needed for Doppler dimmer for getting active.

Noci et al. (1987) reveal other resonance lines, which are expected to have one or both lines enhanced via Doppler-shifted radiation. The ions are 335.407 Å and 360.798 Å of Fe xvi (the first line can be excited by Mg vIII 335.0 Å for a solar wind speed of 364

km/s and the second by Fe xII 359.7 Å (913 km/s) and Si xi 359.0 Å (1500 km/s).

## 5. Conclusions

In this paper we find that the fundamental question of the origin of the fast wind in CHs is intimately connected with the understanding of the plumes and interplumes, starting with the question of their role in the outward flow and their connection with the apparent chromosphere magnetic networks seen as bright points or transient brightening (Tavabi et al., 2018).

DeForest et al. (2001) shown that plumes are both transient and persistent, as they brighten and fade but keep reappearing at the same location: if these recurrent structures are considered a unique objects. Obviously plumes have a long life over which they experience dramatic fluctuations. Their origin is linked to the dissipation of the small-scale magnetic field emerging in Polar Regions and their interaction with the general solar magnetic field leads to the activity inside and around the CH.

In the corona, W-L is primarily due to chromospheric and TR photons resonantly scattered mainly by the coronal neutral H atoms. The radiative emissivity depends on the velocity, with respect to the lower source layers of radiation, of the coronal volume element absorbing and re-emitting the radiation, owing to the Doppler shift. If the radiation emitted by the source consists of an emission line, in the frame of the absorbing hydrogen atoms the relative velocity causes its center to move away from the center of the absorbing profile. The result is a reduced absorption, and therefore a reduced re-emission. Therefore, by measuring this DD effect, it is possible to identify the coronal regions where the wind flows and derive the outflow velocity of its neutral H component (Auchère et al., 2020).

W-L is also sensitive to the DD, and it depends on the outflow velocity of the neutral hydrogen component of the expanding corona. This is because in the frame of reference of the expanding solar wind, the relative wavelength shift of incident chromospheric photons and coronal absorbing profiles causes a dimming of the resonant emission relative to that of a static corona. Hence, in the rest and static corona with zero bulk outflow velocity, the line

profile of chromospheric radiation incident on the corona is centered on the absorption profile of the scattering atom. This case results in a maximum amount of Thomson resonant scattering. The interest is the one where a significant bulk outflow velocity exists in the scattering region (Figure 9). The high-speed outflow decreases the amount of resonant scattering due to the Doppler shift of the incident line radiation as expected in the rest frame of the scattering Fe atoms. As the velocity of the scattering media increases, the scattering probability getting weaker as long as the Doppler shift is large enough so that the amount of resonant scattering approaches zero (Noci et al., 1987).

In addition, DD takes privileged mechanism of formation of most of the coronal lines that are collisionally excited by electron impact in somewhat diluted medium with statistical equilibrium; it also has a minor component radiatively excited by photons originating in background levels. The intensities include two main terms, a collisional  $F_{\text{coll}}$  and a radiative  $F_{\text{rad}}$  component. Among other factors, the latter depends on the outflow speed of the coronal plasma, so the exciting radiation becomes Doppler shifted and the photoexcitation process is less efficient. The radiative term is dimmed by the DD mechanism, and the total intensity decreases (Poletto, 2015). Inferring outflows via the DD mechanism implies the identification of the radiative term line, and the evaluation of the decrease is brought about by the speed of the outward flow. Without entering into a detailed description of the DD mechanism, here we introduced an approximation, as how fast the plasma should move to reproduce the DD effect observationally without making a model to give the velocity and other parameters.

The result gives the unprecedented spatial resolution of total solar eclipse observations for the very high speed outflows from the interplumes region, where the estimated temperature is much higher than plumes ( $20 \times 10^6$  K, Banerjee et al., 2009a), as the plausible sources for the fast solar winds. This achievements should be re-examined by the Multi Element Telescope for Imaging and Spectroscopy (METIS/COR) coronagraph/Solar orbiter particularly during closest approach to the Sun (0.28 AU at the perihelion phase of mission).

Finally, the composite W-L and EUV line-emission diagnostics reveal noticeable uncorrelations between W-L more global, and quasi-stationary structures of Polar Regions with the EUV more dynamical and shorter life-time rays. Further, the eclipse WL images do more advances that are privileged by the best spatial resolutions in both inner and outer parts of corona in the base of a more precise electron density distribution. Accordingly, could permit a better diagnostic about the plausible sources of the fast solar wind. Finally, the connection of WL-PP's with inner parts off-limb EUV emission lines jets have non-perfect correlations; therefore, in some cases, the direct connection was not detectable at all. However, most W-L plumes have counterparts with EUV ray.

### Acknowledgments

The AIA data are courtesy of SDO (NASA) and the AIA consortium, and the eclipse images were provided by J.M. Lecleire and J. Mouette.

### Declarations

Competing Interests The authors declare they have no conflicts of interest.

### References

- Auchère, F., Andretta, V., Antonucci, E., Bach, N., Battaglia, M., Bemporad, A., Buchlin, E., Caminade, S., Carlsson, M., Carlyle, J., Cerullo, J. J., Chamberlin, P. C., Colaninno, R. C., Davila, J. M., De Groof, A., Etesi, L., Fahmy, S., Fineschi, S., Fludra, A., Gilbert, H. R., Giunta, A., & Zouganelis, I. (2020). Coordination within the remote sensing payload on the Solar Orbiter mission. *Astronomy & Astrophysics*, 642, A6. DOI: 10.1051/0004-6361/201937032.
- Banerjee, D., Pérez-Suárez, D., & Doyle, J. G. (2009a). Signatures of Alfvén waves in the polar coronal holes as seen by EIS/Hinode. *Astronomy & Astrophysics*, 501(3), L15-L18.
- Banerjee, D., Teriaca, L., Gupta, G. R., Imada, S., Stenborg, G., & Solanki, S. K. (2009b). Propagating waves in polar coronal holes as seen by SUMER & EIS. *Astronomy & Astrophysics*, 499(3), L29-L32. DOI: 10.1111/j.1365-2966.2009.15279.x.
- Banaszkiewicz, M., Axford, W. I., & McKenzie, J. F. (1998). An analytic solar magnetic field model. *Astronomy and Astrophysics*, v. 337, p. 940-944 (1998), 337, 940-944.
- DeForest, C. E., Lamy, P. L., & Llebaria, A. (2001). Solar polar plume lifetime and coronal hole expansion: Determination from long-term observations. *The Astrophysical Journal*, 560(1), 490.
- Del Zanna, G., Bromage, B. J. I., & Mason, H. E. (2003). Spectroscopic characteristics of polar plumes. *Astronomy & Astrophysics*, 398(2), 743-761. DOI: 10.1111/j.1365-2966.2009.15279.x.
- Gabriel, A. H., Abbo, L., Bely-Dubau, F., Llebaria, A., & Antonucci, E. (2005). Solar Wind Outflow in Polar Plumes from 1.05 to 2.4 R<sub>⊙</sub>. *The Astrophysical Journal*, 635(2), L185.
- Gupta, G. R., Banerjee, D., Teriaca, L., Imada, S., & Solanki, S. (2010). Accelerating waves in polar coronal holes as seen by EIS and SUMER. *The Astrophysical Journal*, 718(1), 11.
- Cho, I. H., Moon, Y. J., Cho, K. S., Nakariakov, V. M., Lee, J. Y., & Kim, Y. H. (2019). A New Type of Jet in a Polar Limb of the Solar Coronal Hole. *The Astrophysical Journal Letters*, 884(2), L38. DOI: 10.3847/2041-8213/ab4799.
- Habbal, S. R., Druckmüller, M., Morgan, H., Scholl, I., Rušin, V., Daw, A., Johnson, J., & Arndt, M. (2010). Total solar eclipse observations of hot prominence shrouds. *The Astrophysical Journal*, 719(2), 1362. DOI:10.1088/0004-637X/719/2/1362.
- Jiao, F., Xia, L., Li, B., Huang, Z., Li, X., Chandrashekar, K., & Fu, H. (2015). Sources of quasi-periodic propagating disturbances above a solar polar coronal hole. *The Astrophysical Journal Letters*, 809(1), L17.
- Koutchmy, S., & Stellmacher, G. (1976). Photometric study of chromospheric and coronal spikes observed during the total solar eclipse of 30 June, 1973. *Solar Physics*, 49, 253-265.
- Koutchmy, S., & Bocchialini, K. (1997). Eclipse WL polar plumes: what is the connection with the disk activity?. In *AIP Conference Proceedings*, 385(1), 137-144). American Institute of Physics.

- Lemen, J.R., Title, A.M., Akin, D.J., Boerner, P.F., Chou, C., Drake, J.F., Duncan, D.W., Edwards, C.G., Friedlaender, F.M., Heyman, G.F., Hurlburt, N.E., Katz, N.L., Kushner, G.D., Levay, M., Lindgren, R.W., Mathur, D.P., McFeaters, E.L., Mitchell, S., Rehse, R.A., Schrijver, C.J., Springer, L.A., Stern, R.A., Tarbell, T.D., Wuelser, J.-P., Wolfson, C.J., Yanari, C., Bookbinder, J.A., Cheimets, P.N., Caldwell, D., Deluca, E.E., Gates, R., Golub, L., Park, S., Podgorski, W.A., Bush, R.I., Scherrer, P.H., Gumm, M.A., Smith, P., Auken, G., Jerram, P., Pool, P., Soufli, R., Windt, D.L., Beardsley, S., Clapp, M., Lang, J., Waltham, N. (2012). The atmospheric imaging assembly (AIA) on the solar dynamics observatory (SDO). *Solar Physics*, 275, 17-40. DOI:10.1007/s11207-011-9776-8.
- Noci, G., Kohl, J. L., & Withbroe, G. L. (1987). Solar wind diagnostics from Doppler-enhanced scattering. *The Astrophysical Journal*, 315, 706-715. DOI: 10.1086/165172.
- Muglach, K. (2021). The Photospheric Footpoints of Solar Coronal Hole Jets. *The Astrophysical Journal*, 909(2), 133. DOI:10.3847/1538-4357/abd5ad.
- O'dwyer, B., Del Zanna, G., Mason, H. E., Weber, M. A., & Tripathi, D. (2010). SDO/AIA response to coronal hole, quiet Sun, active region, and flare plasma. *Astronomy & Astrophysics*, 521, A21. DOI: 10.1051/0004-6361/201014872.
- Pant, V., Dolla, L., Mazumder, R., Banerjee, D., Prasad, S. K., & Panditi, V. (2015). Dynamics of on-disk plumes as observed with the Interface Region Imaging Spectrograph, the Atmospheric Imaging Assembly, and the Helioseismic and Magnetic Imager. *The Astrophysical Journal*, 807(1), 71. DOI:10.1088/0004-637X/807/1/71
- Pasachoff, J. M., Jacobson, W. A., & Sterling, A. C. (2009). Limb Spicules from the Ground and from Space. *Solar Physics*, 260, 59-82. DOI:10.1007/s11207-009-9430-x.
- Poletto, G. (2015). Solar coronal plumes. *Living Reviews in Solar Physics*, 12, 1-67.
- Pucci, S., Poletto, G., Sterling, A. C., & Romoli, M. (2014). Birth, life, and death of a solar coronal plume. *The Astrophysical Journal*, 793(2), 86.
- Samanta, T., Pant, V., & Banerjee, D. (2015). Propagating disturbances in the solar corona and spicular connection. *The Astrophysical Journal Letters*, 815(1), L16. DOI: 10.1088/2041-8205/815/1/L16
- Saito, K. (1965). Polar Rays of the Solar Corona, II. *Publications of the Astronomical Society of Japan*, 17, 1 (1965)., 17, 1.
- Sornette, B., Fort, B., Picat, J. P., & Cailloux, M. (1980). On the physical significance of white light polar plumes in the solar corona. *Astronomy and Astrophysics*, 90, 344-349.
- Sterling, A. C., Moore, R. L., Falconer, D. A., & Adams, M. (2015). Small-scale filament eruptions as the driver of X-ray jets in solar coronal holes. *Nature*, 523(7561), 437-440. DOI:10.1038/nature14556.
- Raouafi, N. E., Harvey, J. W., & Solanki, S. K. (2007). Properties of solar polar coronal plumes constrained by ultraviolet coronagraph spectrometer data. *The Astrophysical Journal*, 658(1), 643.
- Tavabi, E., Koutchmy, S., & Golub, L. (2015). Limb event brightenings and fast ejection using IRIS mission observations. *Solar Physics*, 290, 2871-2887. DOI:10.1007/s11207-015-0771-3.
- Tavabi, E., Koutchmy, S., & Golub, L. (2018). Polar coronal plumes as tornado-like jets. *The Astrophysical Journal*, 866(1), 35. DOI:10.3847/1538-4357/aadc64.
- Teriaca, L., Poletto, G., Romoli, M. and Biesecker, D.A., (2003). The nascent solar wind: Origin and acceleration. *Astrophys. J.*, 588, 566-577.
- Title, A. M., Hoeksema, J. T. Schrijver, C. J., (2006). 36th COSPAR Scientific Assembly, CD ROM 2600, 260, 59-82.
- Van de Hulst, H. C. (1950). On the polar rays of the corona (errata: 11 VIII). *Bulletin of the Astronomical Institutes of the Netherlands*, 11, 150, 11, 150.
- Wang, Y. M., Sheeley Jr, N. R., Socker, D. G., Howard, R. A., Brueckner, G. E., Michels, D. J., Moses, D., St. Cyr, O. C., Llebaria, A., & Delaboudiniere, J. P. (1998). Observations of correlated white-light and extreme-ultraviolet jets from polar coronal holes. *The Astrophysical*

- Journal*, 508(2), 899.
- Wilhelm, K., Dwivedi, B. N., & Curdt, W. (2010). Spectroscopic diagnostics of polar coronal plumes. In *Magnetic Coupling between the Interior and Atmosphere of the Sun* (pp. 454-458). Berlin, Heidelberg: Springer Berlin Heidelberg.
- Wilhelm, K., Abbo, L., Auchère, F., Barbey, N., Feng, L., Gabriel, A. H., Giordano, S., Imada, S., Llebaria, A., Matthaeus, W. H., Poletto, G., Raouafi, N. -E., Suess, S. T., Teriaca, L., & Wang, Y. M. (2011). Morphology, dynamics and plasma parameters of plumes and inter-plume regions in solar coronal holes. *The Astronomy and Astrophysics Review*, 19, 1-70. DOI: ADS. [2011A&ARv..19...35W].
- Ko, Y. K., Stenborg, G., Linker, J., Weberg, M. J., Lionello, R., & Titov, V. (2022). Fine Structures of the Inner Solar Corona and the Associated Magnetic Topology. *The Astrophysical Journal*, 933(1), 95. DOI: 10.3847/1538-4357/ac722c.